www.maajournal.com

Mediterranean Archaeology and Archaeometry
Vol. 22, No 3, (2022), pp. 179-202
Open Access. Online & Print.

DOI: 10.5281/zenodo.7388262

TRANSPORT AMPHORAS FROM GRAVISCA TO THE EASTERN AEGEAN DURING THE GREEK ARCHAIC PERIOD (7th-6th c. BC): A MULTIDISCIPLINARY APPROACH FOR CHARACTERIZATION, MANUFACTURING, PROVENANCE AND TRADE

Andrea Bisciotti*[1], Paola Comodi[2], Maximiliano Fastelli[2], Azzurra Zucchini[2] and Lucio Fiorini[3]

[1]Dipartimento di Fisica e Scienze della Terra, Università degli Studi di Ferrara, Via Saragat, 44122 Ferrara, Italy
[2]Dipartimento di Fisica e Geologia, Università degli Studi di Perugia, Via Pascoli, 06123 Perugia, Italy
[3]Dipartimento di Ingegneria Civile ed Ambientale, Università degli Studi di Perugia, Via G. Duranti, 06123 Perugia, Italy

Received: 14/11/2022
Accepted: 25/112022
**Corresponding author: Andrea Bisciotti (andrea.bisciotti@unife.it)*

ABSTRACT

This paper described a baseline for a multidisciplinary approach to the mineralogical and chemical characterization of eighteen fragments of archaic transport amphoras (7th-6th centuries BC) found at Gravisca archaeological site (Lazio, Italy) attributed to an Eastern Aegean provenance (six from Samos, three from Miletus, three from Chios and three from Klazomenai). The samples have been typed on the evidence concerning archaic manufactory techniques by using X-ray powder diffraction (XRPD) associated with quantitative phase analysis (QPA), optical (OM) and electron microscopy (SEM). Following Inductive Coupled Plasma Spectroscopy (ICP), compositional data analysis has been for the first time applied to selected geochemical proxies combining rare earth elements and selected heavy metals concentration in Hierarchical Agglomerative Cluster (HAC). This innovative approach allows to distinguish different sources of the raw materials used from different geological and geographical areas. Multivariate statistical treatments via Principal Component Analyses (PCA) open the possibility to group the sherds into clusters, comparing the results with the HAC application allowing to validate the methodology. Two distinct centres associated with Samos manufactory appear to be operating during 7 th-6th centuries BC, which could be related to different production periods or even different production areas. The new data concur with a more straightforward historical reconstruction of archaic Poleis manufactory and commercial activity toward Etruria and the Mediterranean and with a new methodological approach to archaeometry.

KEYWORDS: Gravisca, Etruria, transport amphoras, East Aegean, Samos, archaeometry, XRPD, ICP

1. INTRODUCTION

The emporium of Gravisca (white dot in Fig. 1a, exact DMS position: 42°12'46''N 11°42'37''E) is one of the most important ports of antiquity, a crossroad of goods, ideas and people between the East and the West of the Mediterranean, since the end of the 7th century BC to the Roman period. The harbour was situated about ten kilometres from Tarquinia (the ancient Tarkna), one of the most important Etruscan metropoleis. The first settlers, a group of Phocaea sailors from the East Aegean region (West of Turkey) landed here, at the end of the 7th century BC, to exchange goods with the Etruscan natives (Fiorini, 2005; 2015; Fiorini & Torelli, 2017). From this early period, almost until the first part of the 5th century BC, under the protection of the deities of the sanctuary, Gravisca represented an archaic centre of exchange in the Mediterranean area (Torelli, 1977; 1981; Fiorini & Torelli, 2017). During the 6th century BC and almost until the first part of the 5th century BC, many other traders from different Greek Settlements of the Ionia, Attic, and Magna Graecia were attracted here by the opportunity of good affairs (Fiorini, 2005). The largest volume of the exchanged goods was stored inside transport amphoras, the earliest historical consumer packages (Twede, 2002), which are now widely distributed in fragments as archaeological finds in various Mediterranean archaeological sites. During the Archaic period, the different Mediterranean centres producing transport amphoras developed their trademark external morphology and stamped marks (Grace, 1947; Grace, 1953). This ante litteram form of guaranteeing the provenance of wine and oil, together with other 'characteristic' features, has traditionally been used by archaeologists to identify the origin of the transport amphoras. However, several past analyses showed that the relationship between the stamps, shapes and fabrics of amphoras are quite complex. There could be cases where 'characteristic' properties of one class of the amphoras appear in vessels of another type (Whitbread, 1995) hence a careful archaeometric analysis is called into question. Indeed, a multidisciplinary approach for this type of material is widely reported and discussed in the literature (e.g. Okan et al., 2015; Cau Ontiveros et al., 2018). In the present work, eighteen transport amphoras from the Gravisca site were studied (Table 1, Fig. 3, Fig. 4, Fig. 5) through an archaeometrical approach. The samples under analysis were attributed to several possible origins following the archaeological survey by Di Miceli (Di Miceli, 2019). The above-mentioned research, comparing the morphological geometry of the sherds and supported by the well-known reconstruction of the history of Gravisca, attributed the production of the amphoras to Eastern Aegean Poleis (white dots in Fig. 1b), especially Samos (DMS: 37°40'21''N 26°53'21''E), Miletus (DMS: 37°31'50''N27°16'32''E), Chios (DMS: 38°11'41''N26°01'41''E) and Klazomenai (DMS: 38°21'29''N26°46'03''E). In addition to these artefacts a large group of sherds has been related to indigenous Etruscan industries. Following the main geographical provenance, Di Miceli 2019 has point-out specific 'attributes' that allow assigning the amphoras to detailed 'types' that previous research (Py & Py, 1974; Dupont, 1982; 1998; Sezgin, 2004; 2012, Lambrino, 1938) dated back to a rigorous epoch of production. Classical petrographic description of vessels from X-ray powder diffraction associated with quantitative phase analysis, optical and electron microscopy was made according to the basis of previous works (Whitbread, 1995; Lawall, 1995; Jones, 1986). Furthermore, compositional data analysis from Inductive Coupled Plasma Spectroscopy of rare earth elements and selected heavy metals concentration of the ceramic body was applied to Hierarchical Agglomerative Cluster introducing an innovative interpretation of the data that allows distinguishing different sources of the raw materials used from different geological and geographical origins. Multivariate statistical treatments via Principal Component Analyses open the possibility to group the sherds into clusters directly connected to the different provenance, comparing the results with the innovative Hierarchical Agglomerative Cluster application. The research aim is to establish if the archaeological classification and provenance attribution of the amphoras matches with the analytical results that could be obtained using traditional and innovative archaeometric approaches. This is the first time that the Gravisca artefacts undergo specific analysis to reconstruct their provenance. The samples represent every different type of amphora identified within the archeological site (Table 1) for the mentioned Aegean provenance, dated to the 7th and 6th century BC. Samos specimens were selected in twice the number of the others because morphological differences emerged within specimens belonging to the same assigned. As far as the authors know, there are no recent archaeometric studies published for 7th and 6th century BC Eastern Aegean transport amphoras, especially for samples that have been subjected to a detailed archaeological classification.

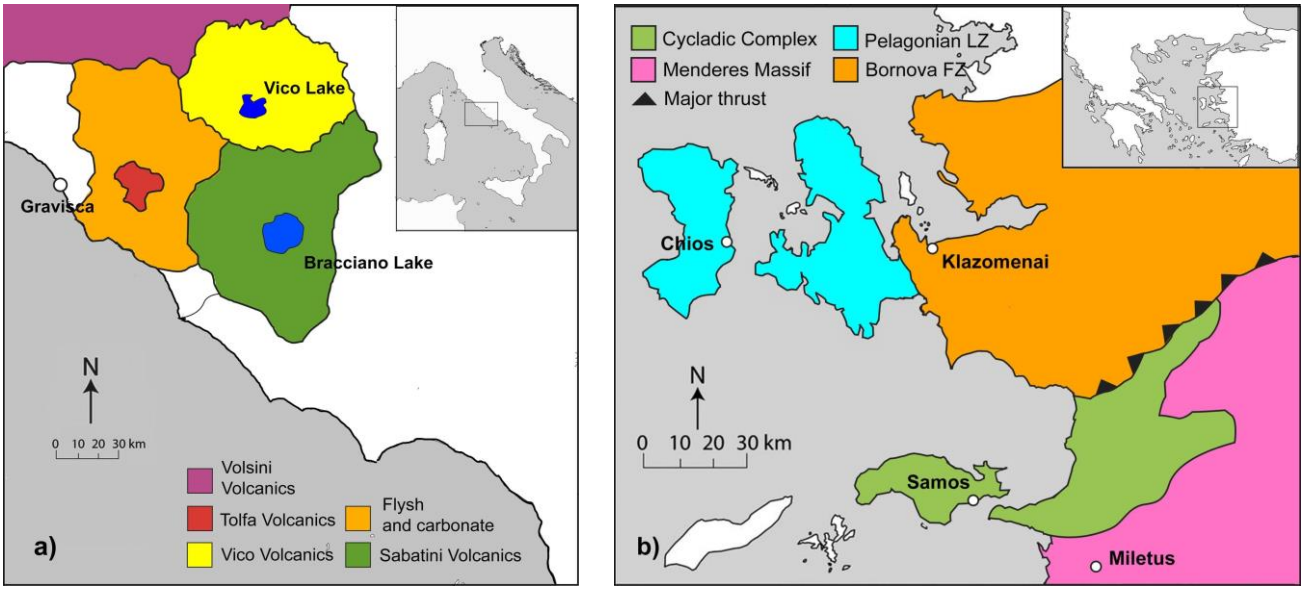

Figure 1. Geographical presumable provenance of archaeological finding under studies: (a) geographical and geological sketch-map of central west Italy (Lazio) with the locations (white dot) of the archaeological site of Gravisca, (b) geographical and geological sketch-map of Eastern Aegean area with the locations (white dots) of the Ionian Poleis (Western Turkey).

2. GEOLOGICAL SETTINGS

Gravisca is part of the Roman Magmatic Province, which originated in the area between the Apennine orogen and the Tyrrhenian coast during the Pleistocene (Marra et al., 2020). The archaeological site lies below tuffaceous hills that are part of a thick pyroclastic plateau formed by the eruptions of large volcanic districts, the Tolfa and Sabatini Volcanics to the South-East and Vico Volcanics to the East (Fig.1a). The geology is dominated by widespread tuff (yellow-red tuff) and pumice from the lower Pleistocene acid cycle of the Tuscan Magmatic Province (Volsini Volcanics) and the K-alkaline sub-saturated silica cycle of the middle to upper Pleistocene of the Roman Magmatic Province (Chiocchini, 2019). The Eastern Aegean is a mosaic composed of different tectonic entities (Fig. 1b). Between them, the Menderes Massif is the predominant geological formation that extends eastwards to the aforementioned Aegean Poleis. The main regional dynamothermal metamorphism occurred from the Late Cretaceous to the beginning of the Miocene, when, after a compressional regime, the Menderes dome collapsed in an E-W direction to form the core rocks and the associated extensional geological formation (Yilmaz, 1997). The Samos Island, belonging to the Cycladic Complex, comprises several Alpine tectonic units and two post-alpine sedimentary basins. An ophiolitic mélange characterises the Samos geology outcrops, where a chaotic mixture of pillow basalts, relict peridotites, serpentinites, clastic sediments and limestones reach a thickness of 200 - 300 m. The mafic and ultramafic blocks within this heterogeneous formation are widespread ranging from a few centimetres to tens of meters (Stouraiti et al., 2017). On the mainland, less than 100 km South-East of Samos, Miletus lies at the base of the Menderes Massif. The Massif is a metamorphic complex cropping out on a large region in the Alpine orogenic belt of Western Anatolia. The area is characterised by acidic magmatism in which the contact between orthogneisses (biotite orthogneiss and leucocratic tourmaline orthogneiss) and thick metaclastic deposit, constitutes the most commonly exposed country-rock (Koralay et al., 2011). Chios island, in the Northern Aegean, is part of the Pelagonian/Lycian zone and, in addition to the Neogene carbonate sediments, a series of small volcanic centres in the northwest and south-east are present. The source magmas have several characteristics comparable to ocean island basalts and resemble subduction-related rocks (Kondopoulou, 2011). Klazomenai, at the Eastern edge of the Bornova Flysch Zone, was formed as a result of subduction-related magmatic activity that produced high-K alkaline products during the Palaeocene-Eocene, which underwent a shoshonitic composition (Agostini, 2010).

3. MATERIALS AND METHODS

3.1. Samples

The transport amphoras analysed come from a series of archaeological excavations conducted, described in (Fiorini, 2015; Fiorini & Torelli, 2017). Three specimens were taken for each group of amphoras classified as Etruscan, Klazomenai, Chios, Mileto and six from Samos. The overall fragments finding of foot and libs from Gravisca excavation is provided in Fig.

2 without counting other ceramic fragments parts (e.g., head, neck, shoulder, walls). Table 1 reports the samples' codes, the provenance area (following the first archaeological classification), the type, the period, and the description of ceramic material by using the Munsell Soil Colour Charts (Munsell, 1975; Zacharias et al., 2018). Each sample can be traced from the archaeological record by its inventory number, also shown in Table 1 (Di Miceli, 2019). For the photographs and drawing of the materials see also Fig.s 3, 4, 5.

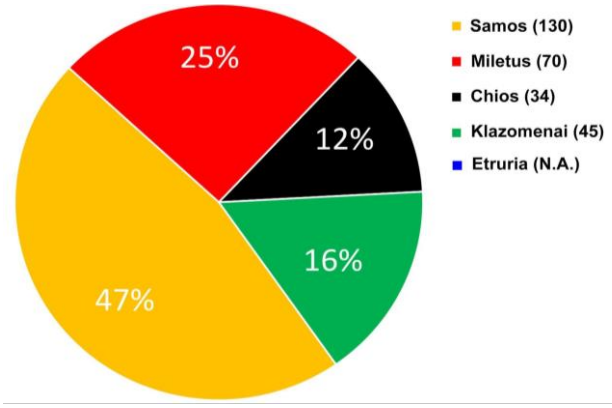

Figure 2. Pie chart with the overall numbers (legend) and percentage (inside graph) of foot and libs from Gravisca excavation (Di Miceli, 2019).

3.1.1. Samos Amphoras

Samos amphoras spread, since the VII century BC, throughout the Mediterranean transporting the oil produced on the island. Can be distinguished by their ceramic colour which varies from red to pink, with an often-greyish core. Present high outward hardness and low porosity with noticeable micas inclusion. Dupont recognizes (Dupont, 1982; 1998) two main types, the first (Table 1: Dupont 23.6.d, Dupont 23.6, Dupont 23.6.f) derives directly from the older classification of the Grace (Grace, 1953) and has an echinus hem, a short and straight neck, an oval belly and a ring-shaped foot. The production of this type is attested between the end of the 7th century to first parts of the 6th century BC. The second type (Table 1: Dupont 1) evolves from the end of the 6th century BC into a pear-shaped body with a shorter neck and a protruding lip, in the bottom a ring-shaped body results in a more rounded profile.

3.1.2 Miletus Amphoras

Miletus amphoras, erroneously recognized at first as a typological evolution of the Samian, were produced from the end of the 7th century BC. In its most ancient and characteristic form (Table 1: Dupont 1), it is characterised not only by the ovoid body, but also by the characteristic banded hem, high and narrow. The amphoras evolved in type 2 during the mid-6th century BC (Table 1: Dupont 2) with a distinctive detail that is the horizontal lines on the neck. Then in the First half of the 5th century BC (Table 1: Dupont 3) there is a progressive elongation of the body and a lowering of the shoulder curve. An essential feature for attributing it to the Milesian production is also the ceramic body, which shows widespread small micaceous inclusions, gold and black, which can be seen reflected under a direct light source.

3.1.3 Chios Amphoras

Chios amphoras produced for the storage and export of its famous wine represent one of the longest-lived productions, covering a period between the 7th and 1st centuries BC. The oldest production dated back at the first half of the 6th century BC (Table 1: Dupont) is characterised by a short cylindrical neck with a thick and protruding rim, arched handles with a flattened biconvex section. The evolution is the A1/A2 of the Lambrino's type (Lambrino, 1938), with a slender neck likewise for the body of the vase which decreases in diameter and lengthens together with the base. Then at the end of the 6th century BC is found the 'Swollen Necked' typology where the shape of the neck widens to form a sort of bulb, meanwhile the body flattens on itself. It has a very wide distribution in both the Mediterranean and Black Sea areas.

3.1.4 Klazomenai Amphoras

The amphoras from Klazomenai present a ceramic body softer and more porous than the other Eastern Aegean amphoras, with evident black and white micaceous inclusions. The external surface presents a painted decoration characterised by a series of brown bands. One was typically positioned around the rim, two along the shoulder and the last in the lower part of the body; vertical lines are present on both handles. Sezgin recognised (Sezgin, 2004; 2012) the production of the last quarter of the 7th century BC for the rounded edge and the cylindrical neck (Table 1: Group II) then an evolution appears with differences concerning the lip, which takes on a "beak" profile and the neck which is more flared (Table 1: Group III).

3.1.5 Etruscan Amphoras

Although Etruscan amphoras have been subjected to multiple classifications, a complete typology of this material class has not yet been established. In the present work (after Di Miceli, 2019) the Py regional attribution is used. Py classification is based on analogous vessels with a provenance from South of Gallia (Py & Py, 1974). The most ancient Etruscan amphorae (Table 1: Py 1/2) can be recognized by an everted edge directly connected to the shoulders with a width and a flat bottom. Types 3A and 3B (Table 1) represent the morphological evolution of the oldest production

and are distinguished by the more elongated body and the truncated cone bottom. Lastly, type 4A (Table 1), the most recent, is characterised by the significant elongation of the rim which takes the shape of a funnel (Py & Py, 1974).

3.2 Analytical Methods

3.2.1 Optical Microscopy and Field Emission-Scanning Electron Microscopy (OM and FE-SEM)

The description of fabric characteristics was performed by transmitted polarized light Optical Microscopy (OM) and Field Emission Scanning Electron Microscopy (FE-SEM) on 30 μm thin sections of the vessel's rims. FE-SEM analyses were performed using a Field Emission Gun Electron Scanning Microscope LEO 1525 with ZEISS AsB (angle-selective backscatter) detector and GEMINI column. Chrome coating (8mm) was applied for SEM observations on the thin section. Thin sections were mounted on stubs with double sided adhesive carbon tape. Measurements were performed on an electron high tension of 5 and 15 kV. The images were captured using secondary electron (SE) and In-lens detectors. The FE-SEM instrument was coupled with Energy Dispersive X-ray Spectroscopy (EDS) system (BrukerQuantax EDS).

Table 1. List of studied samples with sample codes, estimated area of provenance, type, period, chronological classification based on Munsell Soil Color Charts (Munsell 1975; Zacharias et al., 2018) serial numbers related to ceramic colours and original inventory number (Di Miceli, 2019). For all samples a rim fragment. Classification type was made following (Py & Py, 1974(a); Sezgin, 2004; 2012 (b); Dupont, 1982; 1998 (c); Lambrino, 1938 (d)).

Sample code	Estimate area of provenance	Type	Period	Munsell Soil Color Chart	Inventory Number
E3	Etruria	Py 3 A-B(a)	Second half of 6th century BC.	5YR7/6	72/7931
E4	Etruria	Py 4A(a)	Half of 5th to half of 3rd centuries BC.	10YR8/3-7/4	73/21617
E1	Etruria	Py 1/2(a)	First half of 5th BC.	10YR8/3-7/4	78/5870
CL1	Klazomenai	Group III Sezgin(b)	First half of 6th century BC.	5YR6/8	75/6130
CL2	Klazomenai	Group II Sezgin(b)	End of 7th century BC.	7.5YR7/6-6/6	76/11380
CLINC	Klazomenai	Unknown	Unknown	5 YR6/6-6/8	75/11860
M1	Miletus	Dupont 1(c)	End of 7th, first half of 6th century BC.	7.5YR7/6-6/6	75/5797
M2	Miletus	Dupont 2(c)	Second half of 6th century BC.	7.5YR7/6-6/6	75/8946
M3	Miletus	Dupont 3(c)	First half of 5th century BC.	7.5YR7/6-6/6	72/21568
CH1	Chios	Dupont(c)	First half of 6th century BC.	5YR6/8-7.5YR6/6	72/8904
CH2	Chios	A1/A2 Lambrino(d)	Half of 6th century BC.	5YR6/6	75/4349
CH3	Chios	Swollen Necked Lambrino(d)	End of 6th century BC.	7.5YR6/6	76/13248
S1V2	Samos	Dupont 1(c)	End of 6th century BC.	7.5YR6/4-6/6	75/2200
S2V1	Samos	Dupont 1(c)	End of 6th century BC.	7.5YR7/8-6/8	75/14745
S6V6	Samos	Dupont 23.6.d(c)	End of 7th to first parts of 6th century BC.	7.5YR7/6-6/6	16/3855
S7V5	Samos	Dupont 23.6(c)	End of 7th to first parts of 6th century BC.	5YR6/6-6/8	72/20842
S7V7	Samos	Dupont 23.6(c)	End of 7th to first parts of 6th century BC.	5YR7/8-6/8	78/7357
S8V4	Samos	Dupont 23.6.f(c)	End of 7th to first parts of 6th century BC.	7.5YR6/6-6/8	75/21010

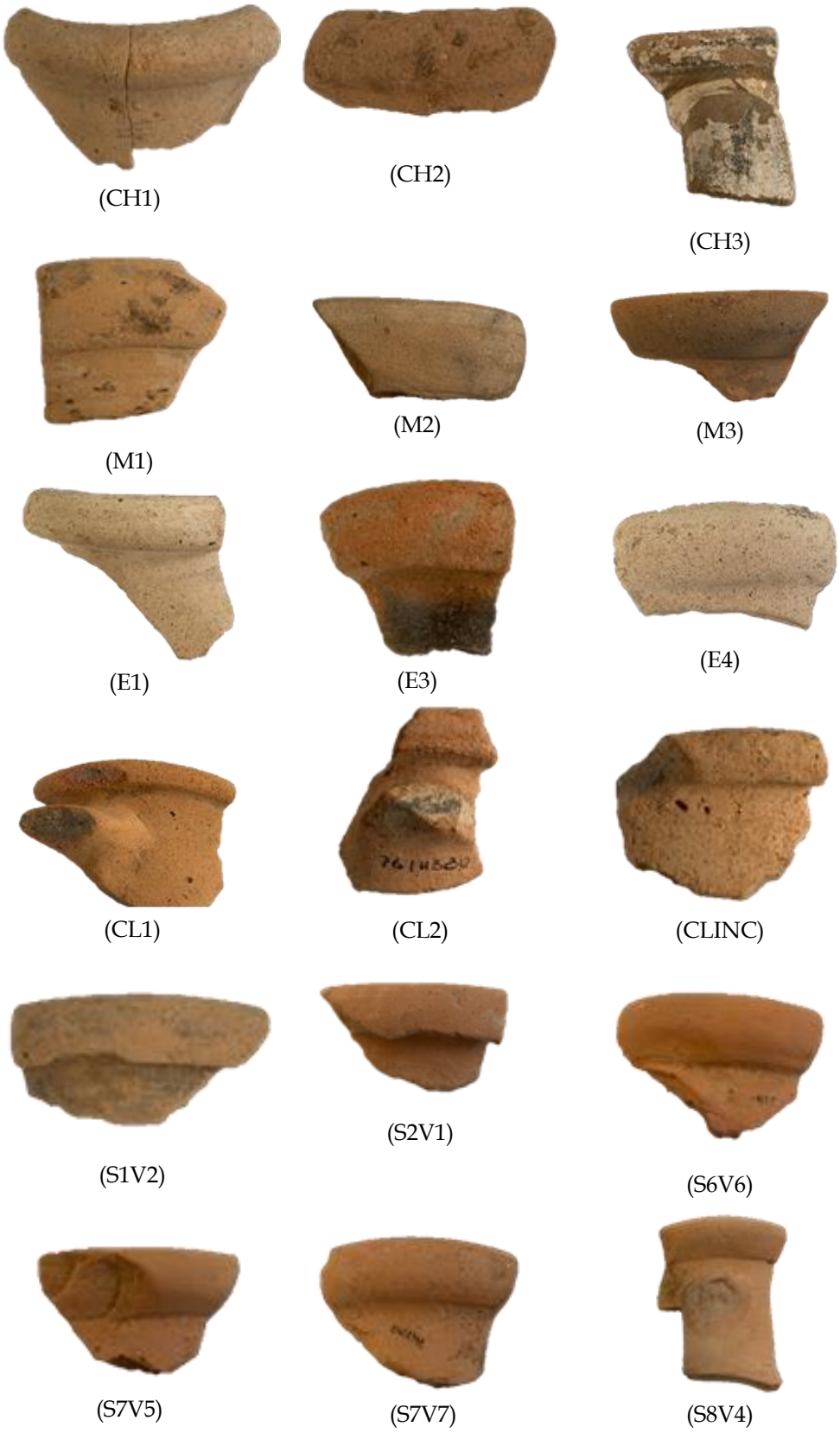

Figure 3. Photographs of transport amphoras jars attributed to different Poleis found at Gravisca and studied in this work.

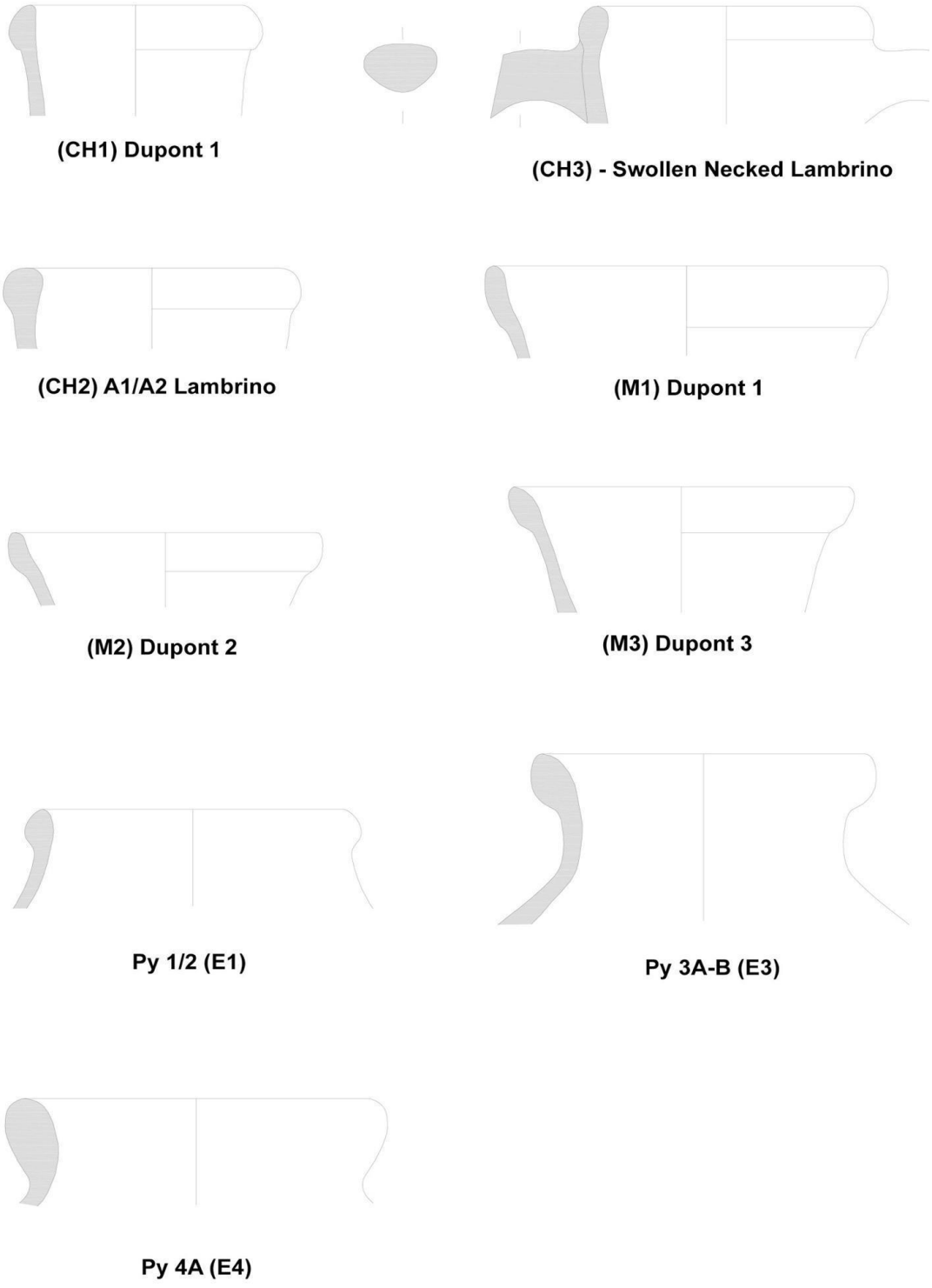

Figure 4. Draws of different types of amphoras section (from Di Miceli, 2019)

Figure 5. Draws of different types of amphoras section (from Di Miceli, 2019)

3.2.2 X-ray Powder Diffraction (XRPD) and Rietveld Analysis

Complementary investigation of mineralogical fabric components was made by XRPD. The used instrument was a Bragg-Brentano θ-2θ diffractometer (Philips PW 1830, CuKα radiation λ= 1.54184 Å, 40 KV and 30 mA) in the 3°- 80° [2θ] range with a step scan of 0.02 [2θ] and a step time of 20 s. The diffraction patterns were qualitatively interpreted by means of X'Pert HighScore Plus 3.0 (PAN analytical) coupled with the Crystal Open Database (COD) library for minerals' profile comparison (Gražulis et al., 2009; 2012; 2015; Merkys et al., 2016; Vaitkus et al., 2021). Quantitative Phase Analysis (QPA) was performed by means of the Rietveld method (Rietveld, 1969) implemented in Material Analysis Using Diffraction (MAUD) software (Lutterotti, 2000) measuring weights percentage consistent with amorphous slightly crystalline ceramic materials (Gualtieri et al., 2014) together with the dispersion factors for neutral atoms. The refined parameters were the background, fitted with a Chebyshev polynomial function, the profile functions (pseudo-Voigt-type), the scale factor, the zero point of the instrument and the lattice constants for each phase. When necessary, the March-Dollase correction (Dollase, 1986) for preferred orientations was applied. The fit accuracy was calculated by the numerical parameter known as R-weighted-pattern (Rwp) reported in Table 2.

3.2.3 Chemical analysis

The chemical characterization of the transport amphoras was made through Inductively Coupled Plasma-Optical Emission Spectrometry (ICP-OES) and Inductively Coupled Plasma-Mass Spectrometry (ICP-MS) to quantify major and minor constituents and trace species, respectively. The used ICP-OES instrument is a Thermo Scientific® iCAP 7000 series, whereas for the ICP-MS analysis a Thermo Scientific® iCAP Q series was used. The chemical analysis allowed the determination of concentration for 50 major, minor and trace elements: CaO, K2O, MgO, Fe2O3, Al2O3, SiO2, Na2O, Y, Pr, Nb, Sm, Eu, Gd, Dy, Ho, Tm, Yb, Lu, B, Ba, As, Sc, Ti, V, Cr, Mn, Cd, Co, Cu, Fe, P, Mo, Ni, Pb, Se, Sb, Sn, Tl, Zn, Zr, Pd, Ag, La, Hf, W, Ge, Ce, Tb, Er, In (Table 3 and Supplementary Materials (S.M.) Table I, II, III, IV). Prior to being analysed, the interior and exterior of archaeological ceramics were abraded to remove adhering soil that would contaminate the sample. The digestion was carried out with HNO3, HClO4 and HF. The determinations were performed in a 1:10 dilution of the solution obtained after the dissolution procedure. The calibration of the instrument was carried out with multi-element standard solutions, HNO3 solution (1M) was used as a blank. For the preparation of the concentrated standard solution, mono-element LabMix24 and CPAchem international standards were used (LM24-CUS-70886, LM24-OP-4003179, C063.2NP.L1, C031.2NP.L1, C025.2NP.L1, C054.2NP.L1, C043.2NP.L1, C016.2NP.L1, C037.2NP.L1, C058.2NP.L1, C021.2NP.L1, C036.5N1FP.L1, C029.2NP.L1, C018.2NP.L1, C068.2NP.L1). The multi-element standard solutions contained all the major and minor chemical species determined by ICP-OES. For the trace element concentrations ICP- MS were used with the above-mentioned calibration method. Instrumental detection limits are in the parts-per-billion range for most elements and precision is within 2–3%.

3.2.4 Multivariate Statistical Analysis

A matrix (NxM) with the 18 samples (N) and 50 concentrations (M) of major (Wt.%) and trace (ppm) elements from ICP-OES and ICP-MS was generated to conduct a multivariate analysis.

The constant sum problem of the composition data was avoided using the Aitchison approach (Aitchison 1982, 1986). Starting from raw data, CoDaPack 2.03 Software (Comas Cufí & Thió i Fernández de Henestrosa, 2011) was used to produce the Compositional Variation Matrix (CVM), which allows the quantification of the total variation (vt) in the data set, and to understand which elements contribute to a greater extent to the observed variability (Buxeda & Kilikoglou, 2003; Aitchison & Egozcue, 2005). Then, the Centered Log Ratio (CLR) transformation of the raw data was applied to the whole set of Rare Earth Elements (REEs) and heavy metals concentration (Cr, Ni, Co, Zn) for agglomerative Hierarchical Clustering (HAC) procedure, using Ward's minimum variance criterion (Ward 1963) available in the CoDaPack 2.03 software. Ward's method, as a hierarchical clustering method, was used to create groups where the variance is minimised. To apply a recursive algorithm under this objective function, the initial distance between individual objects must be proportional to the squared Euclidean distance; after Aitchison transformation in CLR, this condition should be verified. The results have been interpreted in the view of different geological raw materials sources: ultramafic, felsic-mafic and metamorphic origins. Furthermore, the chemical raw dataset was transformed using CoDaPack 2.03 (Comas Cufí & Thió i Fernández de Henestrosa, 2011) in Additive Log Ratio (ALR) using Ge as divisor, and it was analysed through Principal Component Analysis (PCA) using Prism9 Software with GraphPad suite. PCA was applied for data reduction, commonly used in archaeometry studies to highlight the presence of compositional groups between the artefacts. The initial dimensionality of the

data set, equal to the number of chemical species (N), is reduced to n, representing the number of Principal Components (PCs) used. PCs are then calculated as eigenvectors of the covariance matrix of the transformed data, whose eigenvalues represent the variance of the data along with the eigenvector directions. Linear transformation of correlated variables results in an exploratory method in which scores based on the first two variables are plotted either to investigate or display structure in the data (Baxter, 1995).

4. RESULTS

4.1 Fabric description

The description of the thin-section petrography of the amphora's families has been made by means of both OM and SEM with Backscattered Electrons (BSE-SEM). Taking as a base reference the previous Whitbread classification of 7th century BC transport amphoras fabric (Whitbread, 1995). The following characteristics have been highlighted: texture, porosity, micro-mass, matrix, presence and/or absence of amorphous and mineralogical composition with possible identification of index minerals. High-cooking temperatures were inferred by the optical inactivity of thin sections (Medeghini et al., 2020), by the amorphous amount (just only qualitatively estimated) from BSE-SEM imaging of mineral alterations, and from XRPD results like in the case of the presence/absence of calcite, which decomposition temperature occur around 800°C (Aras, 2004).

4.1.1 Etruscan Fabric

Etruscan samples present an optically active micromass with the presence of microcrystal and ochre-brown matrix. Voids and coarse fragments of quartz and feldspar are common and give high porosity (Fig. 6a1). From OM the main minerals observed are feldspars and micas with the sporadic occurrence of calcite and pyroxenes (Fig. 6b1 and 6c1). The E4 sample shows a strongly amorphous ground paste unlike the others, an indication that only this sample was subjected to higher firing temperatures with respect to the other two.

4.1.2 Klazomenai Fabric

Klazomenai specimens are characterised by the presence of a very abundant background paste and fewer blasts of different sizes. The matrix is amber-ochre in colour and porosity is low (Fig. 6a2). From OM observations quartz content is low with a predominance of phyllosilicates. Modulation of the mixture by using tempers is observed by the presence of angular grains of quartz and feldspar used as additives or correctives mainly in CL1 and CL2 samples (Fig. 6b2 and 6c2).

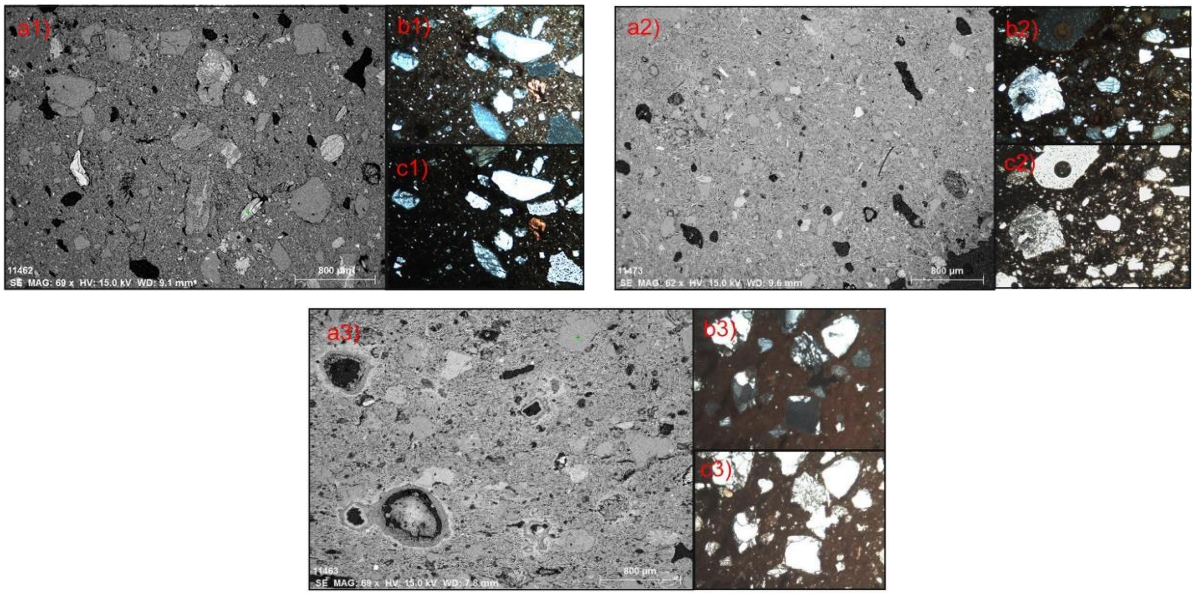

Figure 6. Petrographic and microstructural characteristics of the 30 µm thickness pottery thin section. Etruria sample E4: (a1) BSE-SEM imaging 15 kV magnification 67x, (b1) OM on Crossed-nicol, (c1) OM on Parallel-nicol. Klazomenai sample CL1: (a2) BSE-SEM imaging 15 kV magnification 62x, (b2) OM on crossed-nicol, (c2) OM on parallel-nicol. Chios sample CH1 (a3) BSE-SEM imaging 15 kV magnification 69x, (b3) OM on crossed-nicol, (c3) OM on parallel-nicol. Thin sections highlight texture, porosity, micro mass, matrix, presence and/or absence of amorphous and mineralogical composition.

4.1.3 Chios Fabric

Chios pottery presents a bimodal grain size distribution with several angular clasts (Fig. 6a3). Blasts are medium to large in size composed mainly of quartz and feldspar (orthoclase and plagioclase) with presence of pyroxene (Fig. 6b3 and 6c3). As already observed by Whitbread 1995, are also detected rare serpentinite, sandstone, quartz-biotite schist. Porosity is high due to macro-vughs and thin channels through the paste and around macro-inclusions. Several dissolution voids or dark circular shadows are found within the clay matrix that could be due to calcite dissolution. Microcline, a characteristic metamorphic mineral, can be observed.

4.1.4 Samos Fabric

Samos transport amphoras shows high amounts of amorphous content related to an optically inactive micromass. The matrix is ochre-red-brown in colour. In accordance to Whitbread 1995, inclusion observed mainly comprises dominant to few polycrystalline quartz and white mica, very few to rare orthoclase, plagioclase and limestone (Fig. 7a4). The preferred orientation of mica is well pronounced (Fig. 7b4 and 7c4) and could be related to the use of mechanical potter-wheel. Porosity is low with a predominance of unglazed clay matrix.

4.1.5 Miletus Fabric

Miletus pottery micromass appears optically active with low porosity (Fig. 7a5). The matrix is brown-bordeaux in colour. Moderate degree of isorientation of micas minerals (Fig. 7b5 and 7c5) resulting from the use of mechanical potter-wheel. Grain size distribution is unimodal with medium-small blasts dimension and highly homogenised. Blasts consist mainly of quartz and micas. No detections of additives or correctives, although some components of the skeleton show a certain angularity.

4.2 Mineralogical XRPD assemblage

The XRPD analysis coupled with QPA results, showed substantial homogeneity in the composition of the different ceramic groups in terms of main minerals within the same group. However, the QPA results (reported in wt. % in Table 2) show different mineral assemblages and variability even when comparing samples from the same area. Quartz, feldspars and phyllosilicate are the ubiquitous and dominant mineral phases (>20 wt%) in almost all the analysed specimens (Table 2). Only in Chios amphoras, neither muscovite nor biotite were detected. Biotite was detected only in the Miletus amphoras (M1, M2), whereas in all the other samples muscovite is revealed. Pyroxenes, mainly observed in Chios (CH1, CH2, CH3) and Etrurian samples (E4, E1), are distributed in considerable amounts in several raw materials from similar geographical origin, mainly volcanic. Calcite occurs as an accessory mineral but is also strongly related to the firing temperature reached and its presence it's useful to identify pottery that hasn't been treated at high temperature (~850°C). Furthermore, in Etrurian samples (E3, E1) the presence of analcime could be related to the provenance of the raw materials from the Roman province, where the alteration process of tuff and pumice produce different types of zeolites (Comodi et al., 2014; Novembre et al., 2021). Lastly, hematite cannot be directly linked to an unambiguous geological area or even to geological processes.

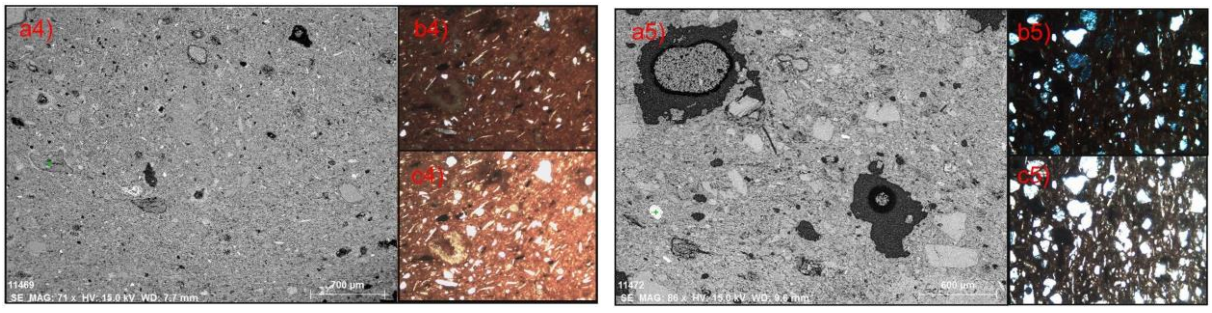

Figure 7. Petrographic and microstructural characteristics of the 30 µm thickness pottery thin section. Samos sample S1V2 (a4) BSE-SEM imaging 15 kV magnification 71x, (b4) OM on crossed-nicol, (c4) OM on parallel-nicol, (a5). Miletus sample M1 (a5) BSE-SEM imaging 15 kV magnification 71x. (b5) OM on crossed-nicol, (c5) OM on parallel-nicol. Thin sections highlight texture, porosity, micro mass, matrix, presence and/or absence of amorphous and mineralogical composition.

Table 2. QPA of the studied samples using the Rietveld method (Rietveld, 1969). Quantities are given in wt. %.

Sample	Quartz	Felds.	Musc.	Biot.	Hem.	Pyrox.	Calc.	Analc.	Rwp
E3	46.00	20.90	29.20	-	-	-	3.50	0.40	14.94
E4	17.10	39.10	15.00	-	-	15.10	13.70	-	10.43
E1	22.80	64.80	1.70	-	-	10.30	-	0.40	13.96
CL1	10.80	76.90	12.30	-	-	-	-	-	15.25
CL2	17.60	61.20	21.10	-	-	-	-	-	11.69
CLINC	17.50	41.70	37.20	-	-	-	3.70	-	14.39
M1	17.60	51.70	15.60	15.10	-	-	-	-	13.16
M2	27.80	55.20	2.90	13.40	0.70	-	-	-	14.52
M3	19.00	55.90	24.90	-	-	-	0.20	-	11.03
CH1	25.60	57.60	-	-	0.60	16.30	-	-	16.85
CH2	46.80	40.60	-	-	0.60	12.10	-	-	12.84
CH3	29.40	41.20	-	-	0.40	29.10	-	-	13.29
S1V2	32.60	67.40	-	-	-	-	-	-	12.3
S2V1	40.20	27.90	31.90	-	-	-	-	-	15.31
S6V6	11.90	62.10	26.10	-	-	-	-	-	10.53
S7V5	12.90	58.90	27.70	-	0.50	-	-	-	12.21
S7V7	18.50	49.10	32.40	-	-	-	-	-	12.12
S8V4	25.60	53.80	20.00	-	0.60	-	-	-	9.3

Where: Felds. = feldspar, Musc. = muscovite, Biot. = biotite, Hem. = hematite, Pyrox. = pyroxene, Calc. = calcite, Analc. = analcime.

4.3 Chemical Analysis

Results of ICP-OES and ICP-MS analyses are given in Table 3 and in S.M. Tables I, II, III, IV. Compositional data are usually recorded as closed data summing to a constant, such as 100%, which precludes the application of standard statistical techniques. In particular, the arithmetic mean, and the variance or standard deviation of individual components do not fit with measures of central tendency and dispersion (Buccianti et al., 2006). Therefore, it is necessary to introduce an alternative as the variation matrix. The compositional variation matrix T of the chemical dataset, derived from ICP analysis (CVM, Fig. 8), provides information on the variability (τ) of compositional data, given in the "ij" element. This matrix, in which all diagonal elements are 0, presents in the off-diagonal elements the variances defined as follow:

$$T = [\tau_{ij}] = [\delta_{ii,jj}] = [\mathrm{var}\{\log(x_i/x_j)\}: i, j = 1, \ldots, D]$$

In the amphoras assemblage analysed the elements that account for a higher variability in the data set are: Na2O (τ.i = 0.70), Ni (τ.i = 0.47), MgO (τ.i = 0.44), K2O (τ.i = 0.43) and Tl (τ.i = 0.38).

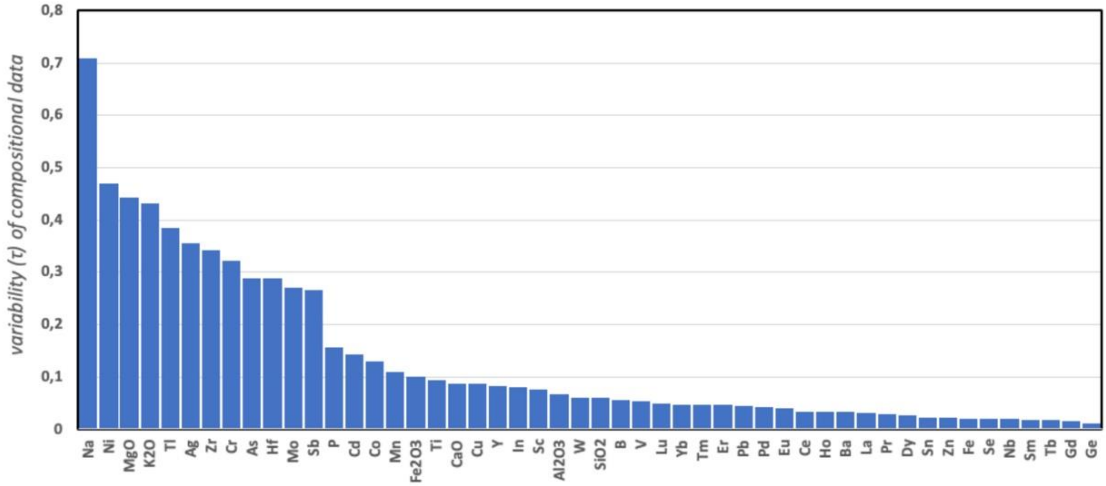

Figure 8. Dataset variability τ.i calculated from the analysed chemical specie

Different enrichments in heavy metals can be related to the chemical composition of the local clays derived from the alteration of the mineral assemblage of the mafic and ultramafic rocks (Otamendi et al., 2016). In particular, soils from weathering of ultramafic/peridotite rocks are typically characterised by high concentrations of four metals: Ni, Cr, Co and Zn (Caillaud et al., 2009; Horen et al., 2014; Nguyen-Thanh et al. 2017). Barone et al. (2004) showed that Cr vs Ni plot could be a good proxy for provenance attributions of pottery since its relevant variation was observed in Greece and Italy. Nickel and chromium scatter-plot can suggest amphoras produced with ultrabasic derived mud (Becquer et al., 2006; Gentili 2014), being these two chemical species generally enriched in olivine/spinel minerals. Furthermore, anomalous concentrations of Ni and Cr are mainly due to serpentine, a typical mineral produced from the weathering of peridotite rocks. From the analysis of whole-rock data (Kierczak et., al 2021), we can observe that without the presence of ultramafic minerals, the average value of Cr and Ni in soils is about 100 ppm respectively. Instead, due to the presence of olivine, clinopyroxene and serpentinite, values of 150 ppm and 300 ppm are reported for Ni and Cr. Examining the Cr vs Ni plot (Fig. 9), we can observe that all the samples from Chios (CH1, CH2, CH3), three samples from Samos (S7V7, S7V5, S6V6) and one sample from Miletus (M3) have a concentration higher than 200 ppm in Cr and Ni. Therefore, these specific samples may be related to an ultramafic geological environment of the raw materials used in the sherds.

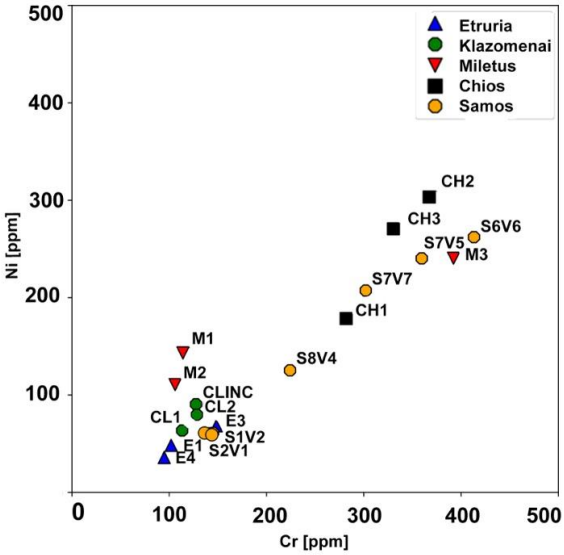

Figure 9. Bi-plot scatter data plot of Cr vs Ni [ppm] plot from the studied samples.

Table 3. ICP-OES chemical analysis of major elements in % wt of oxides.

Sample	CaO	K_2O	MgO	Fe_2O_3	Al_2O_3	SiO_2	Na_2O
E3	4.92	0.85	1.19	5.32	14.19	36.19	3.31
E4	7.00	1.11	2.03	5.83	15.91	39.41	0.49
E1	5.23	1.05	1.73	5.92	15.49	34.17	3.24
CL1	5.96	1.14	1.55	6.46	18.42	40.61	4.81
CLINC	6.26	0.08	0.84	8.93	17.59	35.41	3.40
CL2	5.08	1.12	1.03	7.00	16.47	45.46	4.61
M2	4.54	1.00	1.58	5.89	17.75	41.04	4.19
M1	7.16	1.92	2.92	6.77	18.51	41.63	4.84
M3	7.17	1.11	1.59	8.99	20.70	39.83	0.47
CH3	9.65	0.68	4.56	6.66	14.08	37.22	0.48
CH1	7.40	0.67	3.09	5.97	13.76	40.27	4.74
CH2	6.43	0.47	2.56	6.61	13.96	32.68	4.43
S6V6	6.03	1.09	2.44	10.13	22.78	37.05	3.11
S7V7	6.34	0.17	0.36	7.52	16.85	34.55	0.47
S2V1	7.26	1.53	1.33	6.26	19.07	31.06	3.60
S7V5	6.34	0.18	0.34	8.16	18.46	43.86	0.41
S8V4	7.10	1.37	1.19	6.75	21.06	36.27	4.61
S1V2	8.52	0.70	0.19	6.00	18.97	34.90	4.17

On the other hand, specific REEs have proved that they could be used as a proxy in soils for felsic and metamorphic geological environments (Zaharescu et al., 2017; Frondini, 2014; Henderson, 1984). For example, La and Ce anomalies, can be associated with weathering of granite rock leading to enrichments in the derived soils (Pruysers et al., 1991). Ce can occur as Ce (IV) and Ce (III), where Ce (IV) is less mobile than Ce (III). During weathering processes, Ce (III) is oxidised to Ce (IV) and it either precipitates as either CeO2 or is absorbed by secondary minerals such as Fe/Mn-hydroxides (Han et al., 2019; Zhou et al., 2020). The La values instead, it is a widely used indicator that reflects the degree fractionation extent between HREEs and LREEs (Zhou, 2020). HREEs exhibit higher mobility than that of LREEs in the weathered crust, because as they tend to form complexes with carbonate ligands that have better migration than other complexes (Nesbitt, 1979; Mihajlovic et al., 2019; Vázquez-Ortega et al., 2015). The different migration rates lead to the enrichment of LREE in the upper section and HREE at the lower part of the weathered crust. Diving both species with Yb allows to normalise the data. In conclusion the Ce/Yb values provide information on possible enrichment from granitic derived soils meanwhile high La/Yb ratio refers to the crustal proximity of the derived rock material, while the low La/Yb ratio to a deeper crust source. Ce/Yb and La/Yb (Fig. 10) enrichment are documented for Etruria samples (E1, E2, E3) for Klazomenai (CL2) and Samos specimens (S1V2, S2V1 and S8V4).

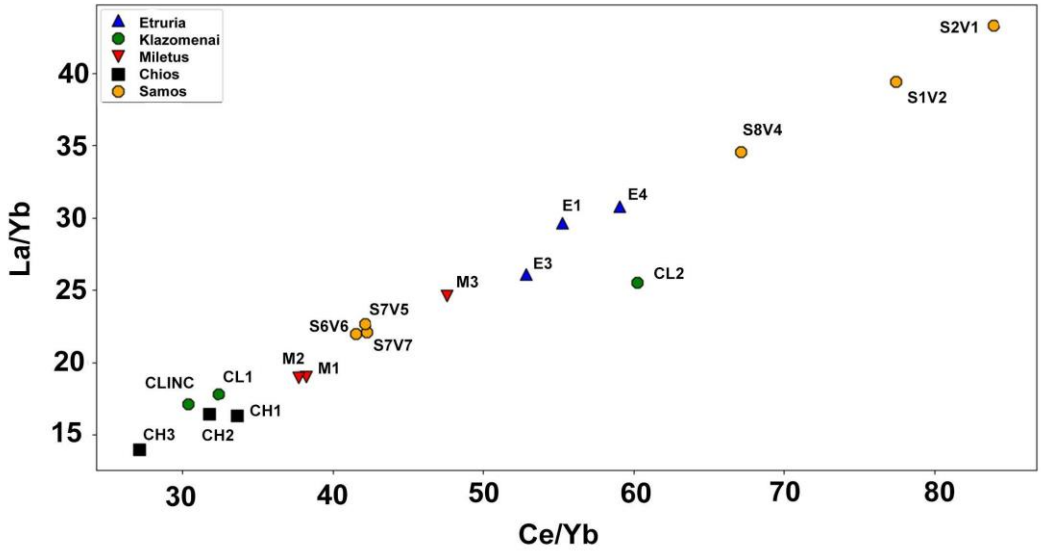

Figure 10. Ce/Yb vs La/Yb bi-plot of the studied samples.

4.4 Multivariate Statistical Analysis

All the values for the different REE concentrations (La, Ce, Pr, Nb, Sm, Eu, Gd, Tb, Dy, Ho, Er, Tm, Yb, Lu) and selected heavy metals (Cr, Ni, Co, Zn) were finally applied to Ward's minimum variance method (Ward, 1963) for the Hierarchical Agglomerative Clustering (HAC) procedure. The dataset consisting of the mentioned chemical species was previously transformed into Centered Log Ratio (CLR). The HAC dendrogram incorporates a "contiguity" relationship between objects in the clustering process (Lebart, 1978; Grimm, 1987; Gordon, 1996). The obtained partition minimises the within-cluster inertia or "error sum of squares". The HAC results are visualised with a graphical dendrogram representation, which also supports model selection and interpretation of the results. The dendrogram results (Fig. 11) provide comprehensive evidence leading to differentiate the geological raw material sources. Two main families were obtained from HAC, in which the samples belonging to groups 1 and 2 are distinguished from those belonging to groups 3 and 4. Group 1 and Group 2 samples are all related to Samos and Chios (S7V7, M3, S6V6, S7V5, CH1, CH2, CH3) and were previously presented as related to an ultra-mafic mineral's soils (Fig. 9). The last two groups contain all the samples that are consequently geochemically different from an ultramafic contest. In this perspective evidence for possible felsic and metamorphic geological environments were already presented for the majority of these samples (Fig. 10). We can observe that within group 3, Klazomenai samples (CL1, CL2, CLINC) are well related to each other, also showing a similarity to those from Miletus (M1, M2). Group 4, on the other hand, contains all the Etrurian samples and three Samos samples (S8V4, S1V2, S2V1) that were already separated from the other Samian specimens in the previous data-plots.

The initial dimensionality of the data set, equal to the number of chemical species concentrations from ICP, is reduced to two variables, representing the number of Principal Components (PCs). The entire data set was transformed in Additive Log Ratio (ALR) using Ge as divisor. The species found in the loading plot (Fig. 12) represent in each of the two directions of the PC axes the greatest variability compared to the original input data set. Following data reduction of the redundant species with a minor impact on the variance in the PC's the loading of dataset accounts for the residual species (SiO2, V, B, Ho, Cr, Na, As, Sb, Fe2O3, Y, Ti, Tl, Mo, Pd, Pr, Zr, Hf and Se) that were used to calculated the PCs values. The chosen methodology wants to maximise the variance inside PCA to enhance the observable differences between the specimens. The chemical species selected after studying the normal distribution of the dataset appear as the most reliable variables, presenting minor outliers.

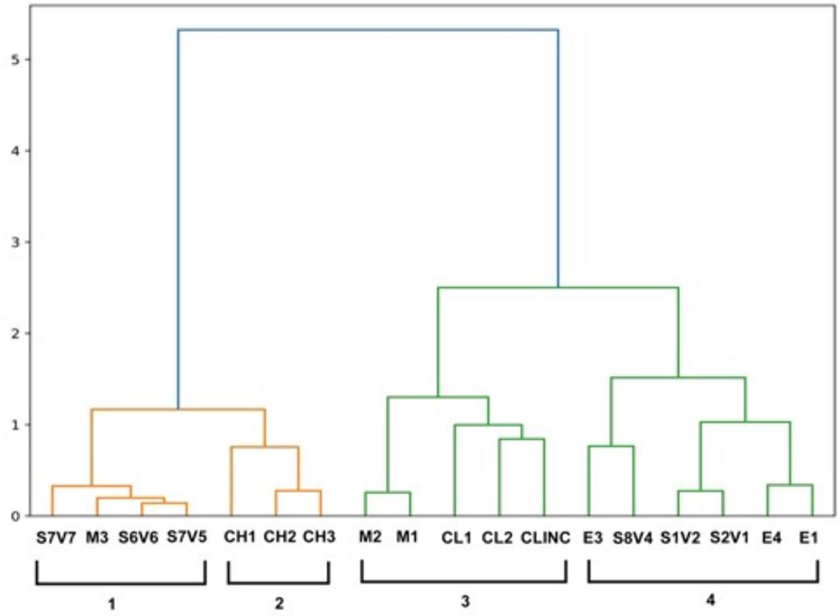

Figure 11. Dendrogram representation of Ward's minimum variance method for agglomerative hierarchical clustering HAC of heavy metal (Cr, Ni, Co, Zn) and REEs concentration (ppm).

Results of the PCA are given in Fig. 13 and allow materials to be referenced with the Euclidean connection distance indicating clusters directly related to the difference in the major and trace chemical concentration of the sample (Baxter, 1995). The PCA plot (Fig. 13) provides evidence of at least five different clusters related to the archaeological amphoras investigated, which are also equivalent to the number of the initial distinct provenance. In this perspective, the present results agree with the main provenance attribution based on morphological type conducted by Di Miceli (2019). Only for the cluster related to the Samian sample (orange points, Fig. 13), it is possible to observe the anomalous presence of the M3 sample, which was previously considered to be of Milesian manufacture. By the present results, considering the QPA and PCA results, it can be concluded that the M3 sample it's of Samian origin. Comparing the clusters resulting from PCA with those of the HAC dendrogram, it was possible to derive substantial consistency in the interpretation of the data. Considering that the chemical species used in the two multivariate methods are almost completely different, the results obtained could give support to the validation of the proposed methodology. In this perspective, the use of the HAC procedure, applying the CLR transformation of heavy metal (Cr, Ni, Co, Zn) and REEs concentration, proves to be a valid proxy for distinguishing the different main geological characteristics of the raw materials used. At least making it possible to clearly distinguish, within the clusters, between ultra-mafic, felsic and metamorphic.

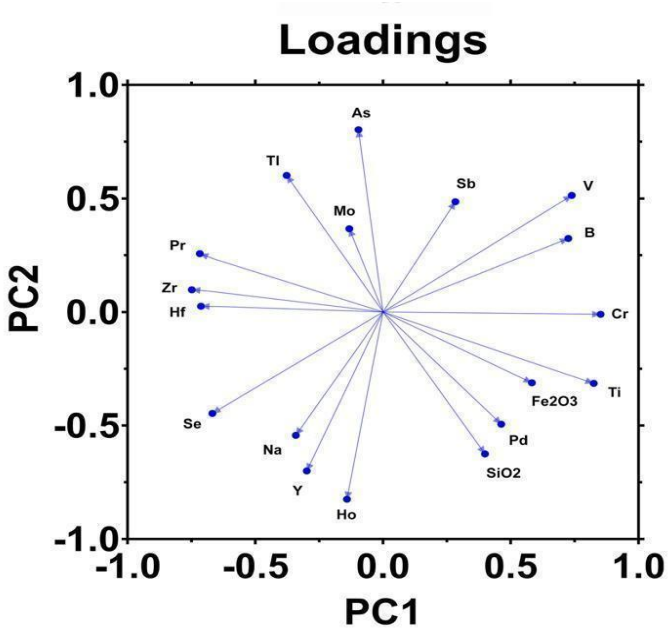

Figure 12. Loadings of different species that account for the variability of PCs. The eigenvectors of the covariance matrix of the transformed data are given together with their eigenvalues that represent the variance of the data along with the eigenvector directions.

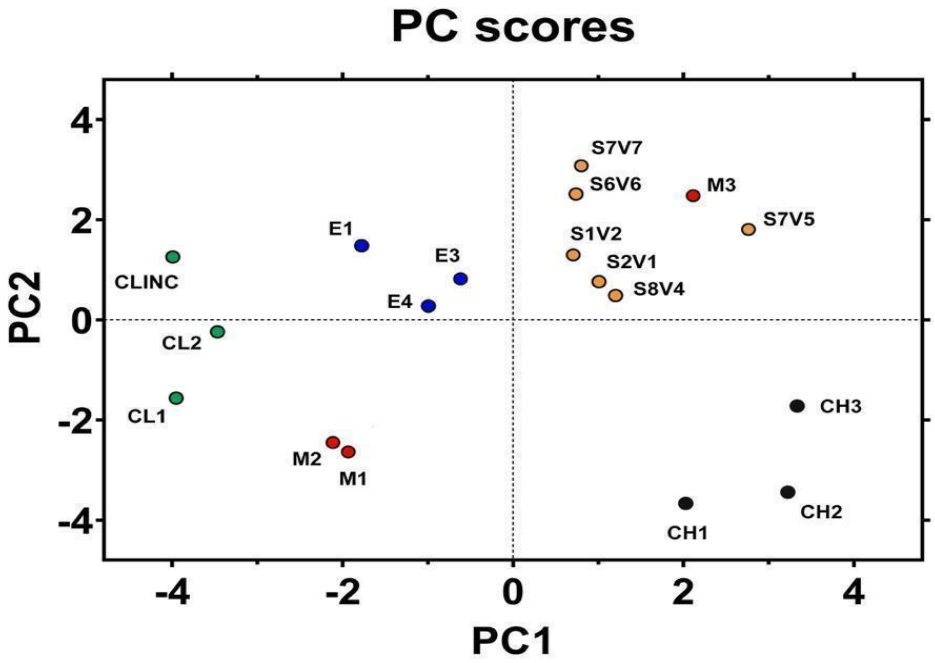

Figure 13. PCA scores plot of studied samples (Klazomenai green points, Etrurian samples blue points, Milesian samples red points, Chios samples black points, Samos samples orange points).

5. DISCUSSION

By combining the results of the tissue characteristics, the mineralogical assemblage and the chemo-mineralogical statistical analysis on the amphora set, the following considerations can be made:

1) Comparing the fabric of transport amphoras Ionian production of 7th-6th centuries BC, Chios, Miletus and Samos amphoras present evidence of a 'standardised manufacture'. The clay, as mainly observed for Samos and Miletus amphoras, is free from impurities that could be the results of soaking processes or by the mining of selected raw materials. The wet clay was frequently worked mechanically using potter wheels, resulting in a more cohesive shape. Firing should then be conducted at high temperature (> 850° C) to produce an extremely resistant ceramic body, as emerged

by the relatively high amount of amorphous components observed with optical microscopy. This aspect was certainly of primary importance considering that transport was often stormy, and the need to avoid rupture of the amphoras was at any cost to be avoided. The presence of coarse aggregate inclusion, in this context, produces 'weak points' that could easily lead to shear rupture resulting in a failure expedition. The technical awareness acquired at that time came from a solid and widespread commercial activity of these Poleis that started in the 7th century BC after their settlement in the Ionian area (Roebuck, 1953). Samos, Chios and Miletus were the first colonies developed after migrations from the Greek area (Hanfmann, 1948) followed in the succeeding century by the foundation of other Poleis on the adjacent coast. Klazomenai and Etruria were developed later in this context, starting their own exporting activity and amphoras production only in 7th-6th centuries BC. Their amphoras production shows an 'experimental manufacturing' approach, mainly observed in the use of coarse temper, lower and heterogeneous firing temperature (often < 850°), and by the absence of mechanical processing of the clay.

2) The mineralogical composition of amphoras displays a similar primary mineral composition, consisting mainly of quartz, feldspar and micas in variable amounts and, when detected, minor contents of calcite, pyroxene, biotite and analcime. Pyroxenes are characteristic minerals of volcanic and metamorphic environments as observed in Chios specimens (CH1, CH2, CH3) and Etrurian samples (E4, E1). The absence of phyllosilicate minerals from Chios samples could be read as evidence of high temperatures reached during the firing process (> 950°C) that resulted in the thermal collapse of the crystal structures. Following OM, the presence of microcline was observed for Chios specimens, and could be used as an index mineral related to a ubiquitarian metamorphic environment, which is also characteristic of the Island of Chios. On the other hand, the presence of calcite in the Etrurian samples results as evidence of a lower firing temperature (around 850°C). Analcime that was found in the Etruria samples, could allow to attribute directly to a provenance from the Tarquinia area, and in general to the Roman area, considering the diffusion of tuff and pumice and the well-known zeolitization processes affecting these rocks in this area (Novembre et al., 2021). Furthermore, the presence of biotite appears to be a characteristic marker of the Miletus samples M1 and M2, whereas it was absent in the M3 sample, the first evidence that the archaeological assignment could be incorrect. The outcrop of orthogneiss biotite in the Miletus area, as reported in the geological map, and the presence of this mineral in the Miletus sherds, could therefore represent strong evidence to define their local provenance.

3) CVM can be used for preliminary assessments of chemical composition variability. Evidence related to either different or analogous material provenance can be inferred. The data reflect the use of different raw materials, in agreement with the presence of various workshops in different geographic areas.

4) The chemical and mineralogical composition of clays is influenced by weathering processes linked to the chemical/mineralogical composition of the parental rock. Assuming that the clays used in ceramic preparation were extracted in the proximity of the production centres, the chemical composition of the sherds should then reflect the geochemistry and mineralogical features of the local regions and thus give key information for the provenance attribution. Every single REE species (La, Ce, Pr, Nb, Sm, Eu, Gd, Tb, Dy, Ho, Er, Tm, Yb, Lu) combined with selected heavy metals concentration (Cr, Ni, Co, Zn) were used in Ward's minimum variance method for HAC procedure with graphic representation in a dendrogram. Cr, Ni, Co, Zn trace elements enrichments have been used as proxies to mark an ultramafic context of the parental rocks associated with secondary index minerals formations. Instead, whole REEs concentration trends were related to a possible contribution for felsic and metamorphic geological environments. Group 1 contains Samian samples dated from the end of 7th to first parts of 6th century BC being part of the Dupont 23 type (S6V6, S7V7, S7V5 and M3 outlier that was in conclusion also associated with a Samian manufactory) presenting a direct connection with Group 2 related to Chios amphoras, related to a metamorphic environment. This geochemical affinity reflects the similar Samos Island geological environment with that from Chios, being both related to "primitive" magmas. The first one has been described by the presence of outcrops of mafic and ultramafic rocks (serpentinite, gabbros) whereas the second for small volcanic centres in where the source magma features are comparable to ocean island basalts. Group 3 contains all the Klazomenai and Miletus specimens (if we accept that for the M3 sample have been provided enough evidence that proves instead a Samos provenance attribution). Group 4 contains all the Etrurian samples and the remaining specimens from Samos that were instead dated to the end of 6th century BC and being part of Dupont 1 type (S1V2, S2V1 except for S8V4). The similarity raised from group 3 and 4 could once again be explained from a similar geological environment, this time associated with a more "evoluted" magmatism, different from the previous ultramafic and ocean island basalts. Miletus geology has been in fact described for an acidic magmatic activity that characterised the Menderes massif unit. If

we then consider the acidic-evolved characters of the Gravisca area, associated with tuff and pumice formation, we could conclude that also for the Samos samples (S1V2, S2V1 and S8V4) it could propose a similar geological environment.

5) Multivariate statistical treatment performed through PCA was useful to compare the provenances provided by archaeological evidence with those from archaeometric analysis maximising the differences in the chemical composition after reading the initial whole data set loading scores values. The results could mainly corroborate the initially assessed provenance distinction of sherds made from Di Miceli 2019, but also add interesting new information. The data from PCA showed that the previous HAC based distinction of the geological environment of raw materials source is still effective in the obtained clusters, providing further evidence of its validity. Two groups connected to different geographic Samos manufactories appear from PCA and also from HAC dendrogram. The anomalous presence of the sample M3 within one of the Samos clusters, which was considered on the basis of morphological characteristics of Milesian manufacture, can be reinterpreted according to the present data has to be considered as one of the artefacts of direct production from Samos.

6. CONCLUSION

In this study, a set of eighteen pottery samples, initially attributed to different production sites based on archaeological evaluations (Etruria, Klazomenai, Chios, Mileto and Samos) were studied from mineralogical and chemical analysis using compositional data analysis elaborated with traditional PCA and an innovative approach based on HAC. Textural and mineralogical descriptions extend the previous classification of Eastern Aegean transport amphoras (Whitbread, 1995; Lawall, 1995; Jones, 1986). Manufacture of transport amphoras appear to be consciously designed to obtain the highest mechanical strength, and this awareness could be also correlated to the amount of commercial exchange of the Poleis from the 7th and 6th century BC with the Gravisca emporium. If we consider the different amounts of fragments finds we can see that Samos and Miletus (47% and 25%) the two leading commercial actors also present the highest 'standardisation' in the ceramic manufactory. Chios production is comparable to those from Samos and Miletus but it is still lacking some degree of expertise like in the selection of the raw materials. A different approach emerged from Klazomenai and from the Etruria manufactory, where several 'experimental' techniques were in use at the time. Chios and Klazomenai were involved during 7th-6th in a limited, or at an early stage, exchange activity (respectively 12% and 16%). The HAC procedure permitted us to compare the obtained data with the estimated provenance related to different geological frameworks. A method that has been validated also from the PCA results. The obtained result was used to verify the archaeological provenance attribution of ceramic materials, e.g. in samples M3 that have been directly associated, by both methods, with the Samos manufacture instead of the incorrect Miletus. Furthermore, two different production centres for Samos amphoras have been discovered, with different geological backgrounds. The first one related to the amphoras of the end of 7th century BC, the second, if we attributed the S8V4 sample to Dupont 1, from the specimens dated at the end of 6th century that were manufactured in a different centre. The first half of the 6th century BC is a period of intense building activity in Samos (Kienast, 1992) which must be related to a general economic growth of the island. If we consider transport amphoras as 'consumer packages', then the need for these artefacts grew until the end of the 6th century BC. From this perspective, the old production centres appeared inadequate to cope with the increase in exchange activity. This led to the foundation of new production centres in the area. The conclusions drawn from the present work clearly show, with a great deal of evidence, that at least from the 7th-6th century B.C. onwards, Samos was the leading poleis in commercial activity in the eastern Aegean area.

CONFLICT OF INTEREST

The authors declare that there is no conflict of interest.

AUTHOR CONTRIBUTIONS

Conceptualization, A.Bisciotti. P.Comodi and L. Fiorini; methodology, A. Bisciotti, P. Comodi, L. Fiorini; software, A. Bisciotti, M. Fastelli; validation, A.Bisciotti, P.Comodi and A.Zucchini.; formal analysis, A. Bisciotti, M. Fastelli; investigation, A. Bisciotti, M. Fastelli; data curation, A. Bisciotti, M. Fastelli; writing—original draft preparation, A. Bisciotti, M. Fastelli; writing—review and editing, P. Comodi, A. Zucchini, L. Fiorini; visualization, A. Bisciotti, M. Fastelli; supervision, P. Comodi, L. Fiorini; project administration, P. Comodi and L. Fiorini; funding acquisition, P. Comodi and L. Fiorini. All authors have read and agreed to the published version of the manuscript.

ACKNOWLEDGEMENTS

In memory of prof. Mario Torelli, discoverer of Gravisca Emporium and winner of the Balzan prize in 2014 whom, as part of the Accademia Nazionale dei Lincei research project "Santuari antichi di area etrusco-laziale: interferenze religiose e culturali", included the foresight study of imported and local transport amphorae found in the excavations of the 1970s. We acknowledged Dr. Francesca Boitani Visentini and Maria Gabriella Scapaticci of the Archaeological Superintendence of Southern Etruria, who allowed this study; Dr. Beatrice Casocavallo, for her active help, Dr. Alessandro Di Michele for the help with the FE-SEM analysis.

REFERENCES

Agostini, S., Tokçaer, M., Savaşçin, M.Y. (2010). Volcanic Rocks from Foça-Karaburun and Ayvalik-Lesvovs Grabens (Western Anatolia) and Their Petrogenic-Geodynamic Significance. *Turkish J. Earth Sci*, 19, 157-183. doi:10.3906/yer-0905-11

Aitchison, J. (1982) Statistical uses of the spatial median. *Journal of the Royal Statistical Society: Series B*, 44 (2), 139-160. https://doi.org/10.1111/j.2517-6161.1982.tb01195.x

Aitchison, J. (1986) *Monographs on statistics and applied probability. The Statistical Analysis of Compositional Data*. London, Chapman and Hall. https://doi.org/10.1007/978-94-009-4109-0

Aitchison, J., & J. Egozcue, J., (2005) Compositional data analysis: where are we and where should we be heading? *Mathematical Geology,* 37, 829–850. https://doi.org/10.1007/s11004-005-7383-7

Aras, A. (2004) The change of phase composition in kaolinite- and illite-rich clay-based ceramic bodies. *Applied Clay Science*, 24, 257–269. https://doi.org/10.1016/j.clay.2003.08.012

Barone, G., Crupi, V., Galli, S., et al (2004) Archaeometric analyses on 'Corinthian B' transport amphoras found at Gela (Sicily, Italy). *Archaeometry*, 46, 553–568. doi: 10.1111/j.1475-4754.2004.00173.x

Baxter, M.J. (1995) Standardization and transformation in principal component analysis, with applications to archaeometry. *Journal of the Royal Statistical Society: Series C (Applied Statistics)*, 44, 513–527. https://doi.org/10.2307/2986142

Becquer, T., Quantin, C., Rotte-Capet, S., et al (2006) Sources of trace metals in Ferralsols in New Caledonia. *European Journal of Soil Science*, 57, 200–213. https://doi.org/10.1111/j.1365-2389.2005.00730.x

Buccianti, A., Mateu-Figueras, G., Pawlowsky-Glahn, V., (2006) *Compositional data analysis in the geosciences: from theory to practice*. London, Geological Society of London. doi:10.1144/GSL.SP.2006.264

Buxeda, J., Kilikoglou, V. (2003) *Total variation as a measure of variability in chemical data sets. Patterns and process: a Festschrift in honor of Dr Edward V Sayre*. In: van Zelst, L., Smithsonian Center for Materials Research and Education, Washington DC, 185–198.

Caillaud, J., Proust, D., Philippe, S., et al (2009) Trace metals distribution from a serpentinite weathering at the scales of the weathering profile and its related weathering microsystems and clay minerals. *Geoderma*, 149, 199–208. doi: 10.1016/j.geoderma.2008.11.031

Cau Ontiveros, M.A., Martínez Ferreras, V., Pecci, A., Mas Florit, C., Fantuzzi, L. (2018) Archaeometric Analysis for Provenance and Content of Roman Amphorae from the Site of Sa Mesquida (Mallorca, Spain). *Mediterranean Archaeology and Archaeometry, vol. 18, num. 2, p. 87-105* 2018.

Chiocchini, U., & Savarese, G., (2019) The Viterbo Hydrothermal System and Its Sustainable Exploitation, Central Italy. *JEPT*, 1(3). doi:10.21926/jept.1903003

Comas Cufí M, Thió i Fernández de Henestrosa S (2011) *CoDaPack 2.0: a stand-alone, multi-platform compositional software*. In: Ecozcue, J.J., Tolosana-Delgado, R., & Ortego, M.I., (ed) "Proceedings of CoDaWork'11: 4th international workshop on Compositional Data Analysis". Barcelona.

Comodi, P., Nazzareni, S., Balic-Zunic, T., Zucchini, A., Hanfland, M. (2014) The high-pressure behaviour of bloedite: A synchrotron single-crystal X-ray diffraction study. *Am. Miner*, 99 (2-3), 511–518. doi: 10.2138/am.2014.4640

Di Miceli A, & Fiorini L (2019) *Le anfore da trasporto dal santuario greco di Gravisca*. Milano, Edizioni ETS.

Dollase, W.A. (1986) Correction of intensities for preferred orientation in powder diffractometry: application of the March model. *Journal of Applied Crystallography*, 19, 267–272. https://doi.org/10.1107/S0021889886089458

Dupont, P. (1998) *Archaic East Greek Trade Amphoras*. In: Cook, R.M., & Dupont, P., (ed) East Greek Pottery. London, 142-191.

Dupont, P., (1982) Amphores commerciales archaïques de la Grèce de l'Est. *La Parola del Passato*, 37, 193–209.

Fiorini, L., (2015) *The Sacred Area of Gravisca. Ethnic Interactions and Faith Beliefs in Comparison*. In: Kistler, E., Öhlinger, B., Mohr, M., Hoernes, M., (ed) Sanctuaries and the Power of Consumption, Sanctuaries

and the Power of Consumption. Networking and the Formation of Elites in the Archaic Western Mediterranean World. Proceedings of the International Conference (Innsbruck 20th–23rd March 2012). Wiesbaden, Harrassowitz Verlag, 205–219.

Fiorini, L., (2005) *Topografia generale e storia del Santuario: analisi dei contesti e delle stratigrafie*. Santo Spirito, Edipuglia srl.

Fiorini, L., & Torelli, M., (2017) *L'emporion arcaico di Gravisca e la sua storia*. In: Govi, E., (ed) La città etrusca e il sacro Santuari e istituzioni politiche. Bologna, Bononia University Press, 255–299.

Frondini, F., Zucchini, A., Comodi, P. (2014) Water-rock interactions and trace elements distribution in dolomite aquifers: The Sassolungo and Sella systems (Northern Italy). *Geochemical Journal*, 48, 231–246. doi: 10.2343/geochemj.2.0301

Gentili, S., Comodi, P., Nazzareni, S., Zucchini, A. (2014) The Orvieto-Bagnoregio Ignimbrite: pyroxene crystal-chemistry and bulk phase composition of pyroclastic deposits, a tool to identify syn- and post-depositional processes. *European Journal of Mineralogy*, 26, 743–756. https://doi.org/10.1127/ejm/2014/0026-2404

Gordon, A.D. (1996) A survey of constrained classification. *Computational Statistics & Data Analysis*, 21, 17–29. https://doi.org/10.1016/0167-9473(95)00005-4

Grace, V. (1953) Wine jars in Pottery of the mid-fifth century from a well in the Athenian Agorà. *Hesperia*, XXII, 101-110.

Grace, V. (1947) Wine jars. *The Classical Journal* 22 (8), 443-52.

Gražulis, S., Chateigner, D., Downs, R.T., et al (2009) Crystallography Open Database – an open-access collection of crystal structures. *J Appl Cryst*, 42, 726–729. https://doi.org/10.1107/S0021889809016690

Gražulis, S., Daškevič, A., Merkys, A., et al (2012) Crystallography Open Database (COD): an open-access collection of crystal structures and platform for world-wide collaboration. *Nucleic acids research*, 40, 420–427. doi: 10.1093/nar/gkr900

Gražulis, S., Merkys, A., Vaitkus, A., Okulič-Kazarinas, M. (2015) Computing stoichiometric molecular composition from crystal structures. *Journal of Applied Aystallography*, 48, 85–91. https://doi.org/10.1107/S1600576714025904

Grimm, E.C. (1987) CONISS: a FORTRAN 77 program for stratigraphically constrained cluster analysis by the method of incremental sum of squares. *Computers & geosciences*, 13, 13–35. https://doi.org/10.1016/0098-3004(87)90022-7

Gualtieri, A.F., Riva, V., Bresciani, A., et al (2014) Accuracy in quantitative phase analysis of mixtures with large amorphous contents. The case of stoneware ceramics and bricks. *J Appl Cryst*, 47, 835–846. https://doi.org/10.1107/S160057671400627X

Han, G., Song, Z., Tang, Y., et al (2019) Ca and Sr isotope compositions of rainwater from Guiyang city, Southwest China: Implication for the sources of atmospheric aerosols and their seasonal variations. *Atmospheric Environment*, 214, 116854. https://doi.org/10.1016/j.atmosenv.2019.116854

Hanfmann, G.M.A (1948) Archaeology in Homeric Asia Minor. *American Journal of Archaeology*, 52, 135–155. https://doi.org/10.2307/500561

Henderson, P., (1984) *Chapter 1 - General Geochemical Properties and Abundances of the Rare Earth Elements*. In: Henderson, P., (ed) Developments in Geochemistry. Oxford, Elsevier, 1–32. https://doi.org/10.1016/B978-0-444-42148-7.50001-0

Horen, H., Soubrand, M., Kierczak, J., et al (2014) Magnetic characterization of ferrichromite in soils developed on serpentinites under temperate climate. *Geoderma*, 235–236, 83–89. https://doi.org/10.1016/j.geoderma.2014.06.026

Jones, R.E., (1986) *Greek and Cypriot Pottery: a Review of Scientific Studies, (Fitch Laboratory Occasional Papers 1*). Athens, British School at Athens.

Kienast, H. J. (1992) Topographische Studien im Heraion von Samos. *Archaöologisher Anzeiger*, 171-213.

Kierczak J, Pietranik A, Pędziwiatr A (2021) Ultramafic geoecosystems as a natural source of Ni, Cr, and Co to the environment: A review. *Science of the Total Environment* 755: 1-18.

Kondopoulou, D., Sen, S., Aidona, E., van Hinsbergen, D.J.J., Koufos, G. (2011) Rotation history of Chios Island, Greece since the Middle Miocene. *Journal of Geodynamics*, 51, 327–338. doi:10.1016/j.jog.2010.07.001

Koralay, R., Candan, O., Akal, C., Dora, O., Chen, F., Satir, M., Oberhansli, R. (2001) The geology and geochronology of the Pan-African and Triassic Metagranitoids in the Menderes Massif, Western Anatolia, Turkey. *Mineral Res. Expl. Bull.*, 142, 69-119.

Lambrino, M.F. (1938) *Les Vases Archaiques d'Hisria*. Bucharest, Fundaţia regele Carol I.

Lawall, M.L. (1995) Transport amphoras and trademarks: Imports to Athens and economic diversity in the fifth century BC. Ph.D. diss. University of Michigan.

Lebart, L. (1978) Programme d'agrégation avec contraintes. *Cahiers de l'Analyse des Données*, 3, 275–287.

Lutterotti, L. (2000) Maud: a Rietveld analysis program designed for the internet and experiment integration. *Acta Crystallogr A*, 56, s54.

Marra, F., Castellano, C., Cucci, L., Florindo, F., Gaeta, M., Jicha, B.R., Palladino, D.M., Sottili, G., Tertulliani, A., Tolomei, C. (2020) Monti Sabatini and Colli Albani: the dormant twin volcanoes at the gates of Rome. *Scientific Reports,* 10, 8666. https://doi.org/10.1038/s41598-020-65394-2

Medeghini, L., Mignardi, S., Di Fusco, G., et al (2020) How Microanalysis Can Be Discriminant on Black Pompeian Wares. *Crystals*, 10, 879. https://doi.org/10.3390/cryst10100879

Merkys, A., Vaitkus, A., Butkus, J., et al (2016) COD:CIF:Parser: an error-correcting CIF parser for the Perl language. *J Appl Cryst*, 49, 292–301. https://doi.org/10.1107/S1600576715022396

Mihajlovic, J., Bauriegel, A., Stärk, H.J., Roßkopf, N., Zeitz, J., Milbert, G., Rinklebe, J. (2019) Rare earth elements in soil profiles of various ecosystems across Germany. *Appl Geochem*, 102, 197–217. https://doi.org/10.1016/j.apgeochem.2019.02.002

Munsell Color (1975) Soil Color Charts, Baltimore.

Nesbitt, H.W, (1979) Mobility and fractionation of rare-earth elements during weathering of a granodiorite. *Nature*, 279, 206–210. doi:10.1038/279206a0.

Nguyen-Thanh, L., Hoang-Minh, T., Herbert, H.J., et al (2017) Development of Fe-rich clay minerals in a weathering profile derived from serpentinized ultramafic rock in Nui Nua massif, Vietnam. *Geoderma*, 308, 159–170. https://doi.org/10.1016/j.geoderma.2017.08.021

Novembre, D., Gimeno, D., Cappelletti, P., Graziano, S.F. (2021) A case study of zeolitization process: "Tufo Rosso a Scorie Nere" (Vico volcano, Italy): inferences for a general model. *European Journal of Mineralogy*, 33, 315–328. https://doi.org/10.5194/ejm-33-315-2021

Okan, E., Atila, C., Akyol, A.A. (2015) The Production of Chios-Style Amphorae at a Ceramic Workshop in Phocaea (Foça). *Mediterranean Archaeology and Archaeometry*, Vol. 15, No 3, 259–276.

Otamendi, J.E., Tiepolo, M., Walker, B.A., et al (2016) Trace elements in minerals from mafic and ultramafic cumulates of the central Sierra de Valle Fértil, Famatinian arc, Argentina. *Lithos*, 240–243, 355–370. https://doi.org/10.1016/j.lithos.2015.11.009

Pruysers, P.A., de Lange, G.J., Middelburg, J.J. (1991) Geochemistry of eastern Mediterranean sediments: Primary sediment composition and diagenetic alterations. *Marine Geology* 100:137–154. https://doi.org/10.1016/0025-3227(91)90230-2

Py, F., Py, M. (1974) Les amphores étrusques de Vaunage et de Villevieille (Gard). *Mélanges de l'école française de Rome*, 86, 141–254. https://doi.org/10.3406/mefr.1974.965

Rietveld, H.M. (1969) A profile refinement method for nuclear and magnetic structures. *Journal of applied Crystallography*, 2, 65–71. https://doi.org/10.1107/S0021889869006558

Roebuck, C. (1953) The economic development of Ionia. *Classical Philology*, 48, 9–16.

Sezgin, Y. (2004) Clazomenian transport amphoras of the seventh and sixth centuries. *Klazomenai, Teos and Abdera: Metropoleis and Colony*, 169–83.

Sezgin, Y. (2012) Arkaik dönem İonia üretimi ticari amphoralar. Istanbul, Ege Yayınları.

Stouraiti, C., Pantziris, I., Vasilatos, C., Kanellopouls, C., Mitropoulos, P., Pomonis, P., Moriz, R., Chiaradia, M. (2017) Ophiolitic Remnants from the Upper and Intermediate Structural Unit of the Attic-Cycladic Crystalline Belt (Aegean, Greece): Fingerprinting Geochemical Affinities of Magmatic Precursors. *Geosciences,* 7, 14. doi: 10.3390/geosciences7010014

Torelli, M. (2016) *Le radici materiali nascoste e le pratiche ideologiche visibili della grande emporìa arcaica greca. In: Sanchirico*, S., Pignataro, F. (ed) "ploutos" e "polis". Aspetti del rapporto tra economia e politica nel mondo greco. Atti dell'incontro internazionale di studi di Roma 2013, Roma, 25-57.

Torelli, M. (1981) *Il commercio greco in Etruria tra l'VIII e il VI secolo a. C*. In: II commercio greco nel Tirreno in età arcaica (Atti del seminario in memoria di Mario Napoli), Salerno, 67–82.

Torelli, M. (1977) Greci e indigeni in Magna Grecia: Ideologia religiosa e rapporti di classe. *Studi Storici*, 18, 45–61.

Twede, D. (2002) Commercial Amphoras: The Earliest Consumer Packages? *Journal of Macromarketing*, 22(1), 98-108. doi:10.1177/027467022001009

Vaitkus, A., Merkys, A., Gražulis, S. (2021) Validation of the crystallography open daTable ase using the crystallographic information framework. Journal of applied crystallography, 54, 661-672. https://doi.org/10.1107/S1600576720016532

Vázquez-Ortega, A., Perdrial, J., Harpold, A., et al (2015) Rare earth elements as reactive tracers of biogeochemical weathering in forested rhyolitic terrain. *Chemical Geology*, 391, 19–32. https://doi.org/10.1016/j.chemgeo.2014.10.016

Ward, J.H. (1963) Hierarchical Grouping to Optimize an Objective Function. *Journal of the American Statistical Association*, 58, 236–244. https://doi.org/10.1080/01621459.1963.10500845

Whitbread, I.K. (1995) *Greek transport amphoras. A petrological and archaeological study*. Athens, British School at Athens.

Kierczak J, Pietranik A, Pędziwiatr A (2021) Ultramafic geoecosystems as a natural source of Ni, Cr, and Co to the environment: A review. Science of the Total Environment 755, 1-18.

Yilmaz Y, (1997) Active Tectonics of Northwestern Anatolia - The Marmara Poly-Project. Hochschulverlag AG, Zurich.

Zacharias, N (2018) Assessment of Chromatic Index in Archaeological Ceramics by Munsell and RGB Novel Contribution to Characterization and Provenance Studies. *Mediterranean Archaeology and Archaeometry*, 18, 175-212.

Zaharescu, D.G., Burghelea, C.I., Dontsova, K., Presler, J.K., Maier, R.M., Huxman. T., Domanik, K.J., Hunt, E.A., Amistadi, M.K., Gaddis, E.E., Palacios-Menendez, M.A., Vaquera-Ibarra, M.O., Chorover, J. (2017) Ecosystem Composition Controls the Fate of Rare Earth Elements during Incipient Soil Genesi. *Scientific Reports*, 7, 43208. DOI: 10.1038/srep43208

Zhou, W., Han, G., Liu, M., et al (2020) Geochemical Distribution Characteristics of Rare Earth Elements in Different Soil Profiles in Mun River Basin, Northeast Thailand. *Sustainability*, 12, 457. https://doi.org/10.3390/su12020457

SUPPLEMENTARY MATERIALS

Table I. ICP-MS chemical analysis of the minor and trace elements in ppm.

Sample	Sc	V	Ti	Cr	Co	Zn	Zr	Mo
E3	10.84	102.61	3280.92	148.39	12.02	42.61	15.85	0,73
E4	12.64	104.55	3106.72	94.86	10.61	46.94	85.43	0.49
E1	13.01	140.10	2828.96	101.98	10.89	44.24	82.74	0.55
CL1	10.15	95.26	2393.13	113.27	11.41	61.62	169.68	0.88
CL2	10.36	121.40	2198.64	128.40	13.55	59.91	130.00	0.76
CLINC	10.10	117.75	2052.25	127.50	17.82	49.23	166.82	0.81
M1	10.06	83.83	3168.09	114.04	11.49	36.22	57.83	0.25
M2	9.94	71.76	3194.44	106.02	10.81	37.81	52.92	0.21
M3	18.35	162.55	3912.55	392.21	25.83	53.90	38.82	1,09
CH1	14.61	96.28	3657.64	281.82	17.08	36.95	19.22	0,20
CH2	13.65	94.10	3619.58	367.22	23.76	42.92	26.88	0,39
CH3	16.27	111.82	3448.41	330.45	22.04	37.67	32.57	0,17
S1V2	14.26	121.23	3875.71	145.05	13.77	48.05	74.37	0,29
S2V1	15.18	139.25	2537.00	140.75	13.16	56.10	62.53	0,33
S6V6	19.47	174.01	4174.23	413.22	27.72	63.84	32.60	0,57
S7V5	17.63	166.12	3728.02	359.52	24.43	53.79	39.02	0.56
S7V7	16.56	164.60	2828.98	301.99	23.79	53.53	31.00	0.60
S8V4	15.61	148.52	4757.14	224.14	16.34	58.78	52.60	1.29

Table II. ICP-MS chemical analysis of the minor and trace elements in ppm.

Sample	Y	B	Ba	As	Mn	Cd	Cu	Fe	P	Ni
E3	10,08	97.99	508.03	7.99	867.47	0.05	21.95	37179.52	662.85	68.27
E4	11.37	120.55	549.21	13.01	751.19	0.11	18.70	40745.26	2205.53	35.77
E1	11.80	125	586.88	25.97	878.96	0.16	49.27	41375	2644.55	48.27
CL1	17.75	109.48	389.34	15.11	1265.40	0.12	23.93	45184.60	968.96	63.51
CL2	14.06	134.05	522.57	32.58	1021.98	0.14	48.16	48939.69	1256.22	79.77
CLINC	20.94	142.75	431.5	25.99	1312.75	0.10	27.16	62482	1386.25	90.5
M1	23.39	110.85	670.64	12.03	841.70	0.12	46.18	47325.11	1401.49	143.19
M2	19.10	133.56	454.40	8.77	622.45	0.10	26.19	41212.03	881.48	110.65
M3	14.16	215.80	506.06	42.34	1196.10	0.11	43.53	62862.33	1126.19	240.48
CH1	12.08	104.34	454.75	4.84	831.82	0.03	26.57	41725.62	388.02	178.51
CH2	10.21	131.84	365.57	5.70	1857.55	0.04	25.40	46223.11	1421.70	303.30
CH3	10.51	129.09	295.91	7.49	1074.55	0.05	41.52	46569.77	657.05	270.68
S1V2	7.67	164.62	488.91	9.03	871.23	0.07	22.03	41929.25	880.42	61.08
S2V1	7.96	158	509.5	19.55	1005.5	0.12	46.81	43762.5	1473.75	60.75
S6V6	14.03	249.12	466.52	31.85	1268.94	0.07	42.53	70842.29	1116.74	262.11
S7V5	11.79	204.76	499.27	33.76	1367.58	0.09	45.59	57054.76	1613.37	240.29
S7V7	10.71	151.99	517.69	33.68	1803.98	0.12	42.53	52562.61	2264.38	207.30
S8V4	7.35	221.92	482.01	16.17	529.56	0.04	48.11	47205.17	1012.81	125.37

Table III. ICP-MS chemical analysis of the minor and trace elements in ppm.

Sample	Pb	Se	Sb	Sn	Tl	Pd	Ag	Hf	W	Ge	In
E3	0.12	1.06	0.34	5.22	0.43	0.12	0.14	0.43	346.33	23.40	0.06
E4	0.16	1.16	0.64	4.94	0.30	0.16	0.13	1.66	324.41	23.53	0.06
E1	0.18	1.38	2.71	5.94	0.48	0.18	0.68	1.78	406.66	26.34	0.06
CL1	0.13	1.73	0.73	9.24	0.58	0.13	0.43	3.87	574.95	23.40	0.08
CL2	0.11	1.31	0.66	6.42	0.48	0.11	0.7	2.79	407.00	26.79	0.07
CLINC	0.14	1.57	0.60	8.25	0.34	0.14	0.21	3.57	405.75	28.45	0.07
M1	0.12	1.3	0.83	8.72	0.60	0.12	0.22	1.12	551.70	23.23	0.08
M2	0.13	1.35	0.93	8.10	0.58	0.13	0.30	1.13	549.54	22.90	0.08
M3	0.13	1.13	2.41	7.36	0.71	0.13	0.09	0.90	431.60	24.81	0.08
CH1	0.12	0.84	0.45	4.13	0.17	0.12	0.18	0.49	204.96	18.12	0.06
CH2	0.14	0.91	0.85	6.60	0.09	0.14	0.09	0.75	178.03	17.07	0.03
CH3	0.15	0.80	0.45	4.55	0.04	0.15	0.14	0.85	171.47	16.54	0.02
S1V2	0.13	1.16	0.67	5.66	0.49	0.13	0.15	1.56	340.40	23.27	0.06
S2V1	0.15	1.16	0.87	6.75	0.64	0.15	0.29	1.25	292.43	24.21	0.08
S6V6	0.13	1.14	2.34	5.95	0.47	0.13	0.18	0.76	410.75	25.31	0.07
S7V5	0.11	0.99	2.09	6.41	0.42	0.11	0.86	0.79	364.76	22.33	0.06
S7V7	0.12	1.04	1.68	6.42	0.65	0.14	0.22	0.70	325.30	21.19	0.07
S8V4	0.15	1.01	0.85	6.90	0.48	0.15	0.28	1.50	385.25	24.70	0.07

Table IV. ICP-MS chemical analysis of REEs in ppm.

Sample	**La**	**Ce**	**Pr**	**Nb**	**Sm**	**Eu**	**Gd**	**Tb**	**Dy**	**Ho**	**Er**	**Tm**	**Yb**	**Lu**
E3	26.33	53.37	5.98	24.31	4.69	0.93	3.77	0.24	2.72	0.45	1.22	0.16	1.01	0.14
E4	34.54	66.26	7.29	28.89	5.13	1.08	3.99	0.25	2.74	0.46	1.31	0.17	1.12	0.16
E1	38.19	71.15	8.65	33.56	6.10	1.24	4.78	0.29	3.26	0.55	1.55	0.20	1.29	0.18
CL1	35.12	63.99	7.24	28.61	8.67	0.80	6.78	0.28	4.68	0.77	2.16	0.28	1.97	0.28
CL2	38.88	91.68	10.54	36.35	6.18	0.75	4.78	0.30	3.35	0.56	1.63	0.22	1.52	0.22
CLINC	37.12	65.99	10.50	36.52	6.71	0.75	5.42	0.36	4.34	0.76	2.26	0.32	2.17	0.32
M1	36.60	72.93	8.66	30.93	6.27	1.04	5.26	0.38	4.61	0.79	2.24	0.30	1.93	0.26
M2	35.70	71.71	7.99	30.45	6.21	1.02	5.19	0.38	4.59	0.79	2.19	0.29	1.88	0.25
M3	31.93	61.72	7.08	27.48	5.40	1.13	4.43	0.29	3.29	0.55	1.54	0.20	1.30	0.18
CH1	22.12	45.60	5.05	20.46	4.13	0.86	3.53	0.25	2.99	0.53	1.54	0.21	1.36	0.18
CH2	21.75	42.14	4.84	20.52	4.22	0.95	3.64	0.24	2.92	0.52	1.49	0.20	1.32	0.19
CH3	18.58	36.03	4.15	17.30	3.61	0.84	3.16	0.22	2.80	0.50	1.48	0.20	1.33	0.19
S1V2	42.04	82.56	8.52	33.01	5.99	1.16	4.55	0.28	2.94	0.46	1.24	0.16	1.07	0.15
S2V1	40.14	77.88	8.20	32.03	5.95	1.16	4.61	0.28	2.94	0.45	1.15	0.14	0.93	0.13
S6V6	32.57	61.57	7.10	28.32	5.61	1.21	4.55	0.30	3.48	0.60	1.68	0.22	1.48	0.21
S7V5	29.94	55.73	6.43	25.90	5.06	1.07	4.09	0.27	3.10	0.53	1.49	0.20	1.32	0.18
S7V7	28.05	53.66	6.12	24.46	4.81	1.03	3.91	0.26	2.97	0.51	1.18	0.19	1.27	0.18
S8V4	36.16	70.26	7.20	28.61	5.21	0.97	3.98	0.25	2.69	0.43	1.17	0.15	1.05	0.14